Slippage and scattering of light pulses in hole-coupled free-electron lasers

G.H.C. van Werkhoven,[1] B. Faatz,[2] and T.J. Schep[1]
[1]*Fundamenteel Onderzoek der Materie Instituut voor Plasmafysica "Rijnhuizen," Postbus 1207, 3430 BE Nieuwegein, The Netherlands*
[2]*Ente per Le Nuovo Tecnologie, l'Energia e l'Ambiente, Dipartimento Innovazione, Settore Fisica, Centro Ricerche Energie Frascati, P.O. Box 65, 00044 Frascati, Rome, Italy*
(Received 17 May 1994)

The synchronous interaction between a light pulse and a pulsed relativistic electron beam in a hole-coupled resonator free-electron laser (FEL) is investigated. The spatial structure of the light pulse inside the cavity and the fraction of power lost through the aperture are strongly influenced by the overlap between the light and the electron beam pulses, both in the transverse and in the longitudinal directions. The pulse shape is determined by the competition between power loss and scattering at the aperture, by the gain due to the resonant interaction with the electrons, and by the slippage with respect to the electron pulse. At the back of the optical pulse, where the main interaction with the electron pulse occurs, gain and the associated focusing are dominant. The front of the optical pulse tends to overtake the electrons and will finally propagate in vacuum. In this front region of the pulse, the on-axis field intensity is reduced only due to scattering. The influence of these competing mechanisms on the intracavity field distribution and the extracted power is analyzed. The full spatial structure of the optical pulse is taken into account, whereas the electrons are considered to move in a density averaged ponderomotive potential. The emittance and betatron oscillations of the electron beam are included insofar as they lead to a variation of the beam envelope. The phenomena are demonstrated numerically for FEL parameters close to those of the free-electron laser for infrared experiments.

PACS number(s): 41.60.Cr, 52.75.Ms, 52.35.Mw

I. INTRODUCTION

The free-electron laser (FEL) is a versatile source of coherent radiation, opening up many new applications because of its high output power and wide range of tunability [1]. In this paper, a resonator FEL is considered, such as the free-electron laser for infrared experiments (FELIX), which operates with a pulsed electron beam and in which an on-axis aperture is used to extract the radiation from the cavity [2]. Compared to other outcoupling schemes, such as a Brewster plate, hole coupling provides a broadband extraction of radiation.

In a resonator FEL, multiple round-trips are required for the optical field to reach saturation. During each round-trip, the radial profile is influenced by two counteracting processes. On the one hand, power is lost through the aperture which tends to reduce the field intensity on axis. This will be partially compensated by scattering of the electromagnetic field in subsequent reflections on the mirrors [3]. On the other hand, the optical field, in particular on axis, is amplified by the resonant interaction with the electron beam. Thus the transverse profile of the radiation alters from pass to pass [4,5].

The overlap between the radiation and the electron pulses in the longitudinal direction is determined by their difference in velocity, the synchronization, and the gain. The pulses are synchronized when the round-trip time of the optical pulse matches the repetition rate of the electron pulses, such that they overlap completely at the entrance of the undulator. Due to the exponential character of the amplification process in the linear regime [6], the signal is largest at the back of the optical pulse. This means that the light pulse is effectively slowed down. When the length of the electron pulse is comparable to the slippage length, the longitudinal overlap between the pulses is reduced. This lethargy effect decreases the pulse-averaged gain [7]. The gain can be restored by shortening the laser cavity. This desynchronization of the cavity leads to an effective synchronization of the light and the electron pulses, which holds for many round-trips as long as the gain is sufficiently large. During this phase, gain dominates over losses and scattering and determines the transverse structure of the optical field.

When the laser reaches saturation, the effective velocity of the light pulse will increase. The pulse begins to overtake the electrons and will eventually run ahead of the electron pulse. As a consequence, the radial profile of the light pulse will finally be dominated only by power loss and scattering at the aperture. It will be shown that the resulting radial structure yields a "screening" of the mirror aperture. Behind this pulse, a second pulse will grow as in the linear phase. Upon reaching saturation, this peak will overtake the electrons and the cycle starts again.

This process implies that the intracavity field distribution consists of pulses tied to the electrons and of freely propagating pulses. These contributions have an entirely different transverse structure. For long wavelengths, the radial profile of the light pulse is mainly determined by

 ©1994 The American Physical Society

transmission loss due to a finite mirror size.

In recent years, considerable effort has been put forward in the development of simulation codes and of analytical methods describing a wide range of phenomena. For instance, the generation of sideband modes and slippage related effects such as superradiance and laser lethargy [8,9] can be explained by a time dependent, spatially one dimensional model [10]. Several spatially three dimensional models [11–17] include gain-induced focusing of the optical field and describe a realistic electron beam by solving the complete set of the electron equations of motion. However, most of them do not include finite pulse effects.

In order to investigate the combined influence of the forementioned effects, a model that is suitable for the investigation of pulse propagation in a hole-coupled resonator FEL is presented in Sec. II. The radiation field is expanded into a set of transverse vacuum modes. Unlike the forementioned three dimensional models, only the averaged transverse motion of electrons is accounted for by treating the electrons as moving in a density-averaged, ponderomotive potential. "Warm" beam effects, such as emittance and betatron oscillations, are included insofar as they lead to a variation of the beam envelope. The model is valid as long as the transverse gradient of the optical field over the electron beam is small. Solutions are obtained with a computational effort comparable to a spatially one dimensional model. In Sec. III, the model is applied to an axisymmetric resonator configuration using an on-axis hole for power extraction. Numerical results, demonstrating the combined effect of slippage and of the radial mode structure on the energy density distribution of the radiation pulse, are presented in Sec. IV. Section V summarizes the conclusions.

II. DESCRIPTION OF THE MODEL

The discussion is restricted to the Compton regime of FEL operation. The undulator is either helical or planar, with strength $A_u(\boldsymbol{x})$ and wave number k_u, and consists of N_u periods. The radiation field is assumed to be dominated by a single longitudinal mode $A_r = u\exp[i(k_0 z - \omega_0 t)]$, where $\omega_0 = ck_0$, such that the complex amplitude u is slowly varying in both time and space. The potentials and momenta are normalized to units of e/mc and mc, respectively.

The starting point for the description of the model is the paraxial wave equation

$$\left\{\nabla_\perp^2 + 2ik_0\left[\left(1-\frac{v_{\rm pon}}{c}\right)\partial_{\bar z} + \partial_z\right]\right\}u(\boldsymbol{x},z,\bar z) = \mathcal{S}(\boldsymbol{x},z,\bar z), \quad (1a)$$

which can be derived from Maxwell's equations under the assumptions that the radiation field propagates mainly along the z axis and that its spectral width remains small. To emphasize the pulsed character, the position in both the optical and the electron pulses are labeled by the coordinate $\bar z = z - v_{\rm pon}t$, where $v_{\rm pon} = \omega_0/(k_0+k_u)$ is the phase velocity of the ponderomotive wave. The reason for this is that the electrons have a natural tendency to slow down the radiation pulse in the exponential gain regime and that their velocity is close to $v_{\rm pon}$.

The source term $\mathcal{S}$ is of discrete nature and is averaged over a ponderomotive wavelength $\lambda_{\rm pon} = 2\pi/(k_0+k_u)$ in the coordinate $\bar z$ in order to be consistent with the slowly varying amplitude approximation

$$\mathcal{S}(\boldsymbol{x},z,\bar z) = -f_B^2\frac{\omega_p^2}{c^2}\mathcal{X}(\bar z)\frac{1}{N_{\bar z}}\sum_{i=1}^{N_{\bar z}}\delta(\boldsymbol{x}-\boldsymbol{x}_i)A_u(\boldsymbol{x}) \times e^{-i\psi_i}\left[1-\frac{\delta\gamma_i}{\gamma_r}\right](z,\bar z), \quad (1b)$$

where $\psi = (k_0+k_u)z - \omega_0 t$ is the ponderomotive phase and $\delta\gamma = \gamma - \gamma_r$ is used to denote the electron energy rather than γ itself. The resonant energy γ_r is the energy at which the associated longitudinal velocity $c\sqrt{\gamma_r^2-\mu_e^2}/\gamma_r$ equals the velocity of the ponderomotive wave $v_{\rm pon}$. Here μ_e^2 is the effective mass of a warm electron beam which will be defined later, $\omega_p^2 = e^2 n_0/\epsilon_0 m\gamma_r$, n_0 is the peak density in the electron pulse, and f_B is the usual function which arises from averaging the equations over an undulator period [1]. The longitudinal electron density profile is given by

$$\mathcal{X}(\bar z) = \frac{1}{n_0}\frac{N_{\bar z}}{\lambda_{\rm pon}}, \quad (2)$$

where $N_{\bar z}$ is the number of electrons within a $\bar z$ segment of size $\lambda_{\rm pon}$. As can be shown from the electron equations of motion, $N_{\bar z}$ is approximately constant for all values of the energy detuning of practical interest. This implies that besides the radiation pulse, the electron pulse also may be thought of as being divided into $\bar z$ segments of length $\lambda_{\rm pon}$.

The transverse behavior of the radiation field is modeled by decomposing the field into a complete set of transverse basis functions Ψ_{nm} with $(z,\bar z)$ dependent coefficients

$$u(\boldsymbol{x},z,\bar z) = \sum_{n,m} u_{nm}(z,\bar z)\Psi_{nm}(\boldsymbol{x},z,\bar z). \quad (3)$$

The basis functions Ψ_{nm} satisfy the homogeneous wave equation and are orthogonal with respect to integration over the *transverse* coordinates. The practical applicability of such an expansion lies in the fact that basis functions exist which satisfy the natural boundary conditions of the cavity mirrors of interest [18]. Substitution of Eq. (3) into Eq. (1) leads to a set of differential equations for each of the coefficients u_{nm} that are coupled through the source term

$$\left[\left(1-\frac{v_{\rm pon}}{c}\right)\partial_{\bar z} + \partial_z\right]u_{nm}(z,\bar z) = \frac{1}{2ik_0}\frac{1}{w_{nm}^2}\int d^2\boldsymbol{x}\ \Psi_{nm}^*\mathcal{S}\ (z,\bar z), \quad (4)$$

where the transverse cross section $w_{nm}^2 = \int d^2\boldsymbol{x}|\Psi_{nm}|^2$ is the normalization factor and an asterisk denotes complex conjugation. This result can also be obtained from Eq. (1) using a Green's function method or from the Huygens integral in the Fresnel approximation [19,20].

The electron trajectories, given by the well known six dimensional equations of motion [21], are calculated in a way which can be viewed upon as a compromise between a fully three dimensional (3D) description and a thin electron beam model in which the electrons experience only the on-axis radiation and undulator fields. This is achieved by taking into account only the *averaged* transverse motion of the electrons rather than calculating each individual electron separately. The main assumption is that the transverse dependence of the electron beam can be described by a Gaussian density profile

$$n(\boldsymbol{x}, z, \bar{z}) \simeq n_0 \mathcal{X}(\bar{z}) \frac{e^{-[x^2/2X^2 + y^2/2Y^2]}}{2\pi XY}. \tag{5}$$

Here $X(z,\bar{z}) = \sqrt{\langle x^2 \rangle}$ is the transverse profile of the electron pulse in the x direction. The brackets

$$\langle x^2 \rangle = \int d^2\boldsymbol{x}\, x^2\, n(\boldsymbol{x}, z, \bar{z}) \Big/ \int d^2\boldsymbol{x}\, n(\boldsymbol{x}, z, \bar{z}) \tag{6}$$

denote a density average over the transverse dimensions of a $\bar{z}$ segment in the electron pulse. The electron density is assumed to be constant over a segment, as mentioned earlier. The z dependence of the beam envelope X is governed by the focusing effect of the undulator and the natural divergence of the beam due to a finite emittance. The undulator strength is approximated by $A_u^2(\boldsymbol{x}) \simeq A_{u0}^2(1 + k_x^2x^2 + k_y^2y^2)$, where the second and the third term in the parentheses are small compared to unity. This describes an undulator with a linear focusing force. The values of k_x and k_y depend on the geometry of the undulator, i.e., $k_x = k_y = k_u/\sqrt{2}$ and $k_x = k_u$, $k_y = 0$ in the case of a helical and a planar undulator, respectively. It can be shown that X satisfies the differential equation [22] $\partial_z^2 X + \kappa_{\beta x}^2 X - (\epsilon_x/4\pi\gamma_r)^2 X^{-3} = 0$, where $\kappa_{\beta x} = A_{u0}k_x/\gamma_r$ is the betatron wave number and $\epsilon_x(\bar{z}) = 4\pi[\langle x^2\rangle\langle P_x^2\rangle - \langle xP_x\rangle^2]^{1/2}$ is the normalized emittance of the electron pulse. To obtain this result, the small variation of the longitudinal momentum $\gamma\beta_z$ in the equations of transverse motion is neglected such that they can be solved independently from the longitudinal motion. The differential equation can be solved exactly with the result [23]

$$X(z,\bar{z}) = X_0(\bar{z})[1 - (1 - r_{\beta x}^2)\sin^2(\kappa_{\beta x} z)]^{\frac{1}{2}}, \tag{7}$$

where $X_0(\bar{z})$ is the minimum spot size at $z = 0$ and $r_{\beta x}(\bar{z}) = (\epsilon_x/4\pi A_{u0}k_x X_0^2)$ determines the amplitude of the betatron motion for each segment in the electron pulse. A similar equation describes the evolution of the envelope Y in the y direction. The case $r_{\beta x}^2 = r_{\beta y}^2 = 1$ corresponds to a matched beam.

The averaged transverse motion is taken into account by application of density average Eq. (6) to the source term and to the longitudinal equations of motion. Since all radial profiles are known, the averages can be calculated analytically. The wave equation can be written as

$$\left[\left(1 - \frac{v_{\mathrm{pon}}}{c}\right)\partial_{\bar{z}} + \partial_z\right] u_{nm}(z,\bar{z}) = if_B^2 \frac{\omega_p^2 A_{u0}}{c^2 2k_0} \frac{I_{nm}^*}{w_{nm}} \mathcal{X}(\bar{z}) \frac{1}{N_{\bar{z}}} \sum_{i=1}^{N_{\bar{z}}} e^{-i\psi_i} \left[1 - \frac{\delta\gamma_i}{\gamma_r}\right] (z,\bar{z}) \tag{8}$$

and the average longitudinal equations of motion for each electron in a $\bar{z}$ segment of the electron pulse are given by

$$\frac{d\psi}{dz} = \frac{\omega_0}{c}\frac{\mu_e^2}{\gamma_r^3}\left[\delta\gamma\left(1 - \frac{3}{2}\frac{\delta\gamma}{\gamma_r}\right) + \frac{\gamma_r A_{u0}}{2\mu_e^2}\sum_{n,m}\left(I_{nm}u_{nm}e^{i\psi} + I_{nm}^*u_{nm}^*e^{-i\psi}\right)\right], \tag{9a}$$

$$\frac{d\delta\gamma}{dz} = i\frac{\omega_0}{2c}\frac{A_{u0}}{\gamma_r}\sum_{n,m}(I_{nm}u_{nm}e^{i\psi} - I_{nm}^*u_{nm}^*e^{-i\psi})\left(1 - \frac{\delta\gamma}{\gamma_r}\right), \tag{9b}$$

where the function $I_{nm}(z,\bar{z}) = \langle(1 + k_x^2x^2 + k_y^2y^2)\Psi_{nm}^*\rangle$ is used to denote the density average. The terms proportional to $\delta\gamma/\gamma_r$ and the second term within the square brackets in Eq. (9a) are taken into account since they influence the growth rate of the radiation in the linear regime [6]. The quantity $1 + A_u^2 + |\boldsymbol{P}_\perp|^2$, which enters the non-density-averaged longitudinal equations, is an approximate constant of motion for each electron. Upon averaging over the density, it can be expressed in terms of the electron beam envelope and emittance

$$\langle 1 + A_u^2 + |\boldsymbol{P}_\perp|^2\rangle = 1 + A_{u0}^2[1 + k_x^2X_0^2(1 + r_{\beta x}^2) + k_y^2Y_0^2(1 + r_{\beta y}^2)] \equiv \mu_e^2 \tag{10}$$

and is used to define the effective mass μ_e^2 of a warm electron beam. The system of averaged equations (8) and (9) can be solved numerically with a computational effort comparable to a spatially 1D model.

The justification of the assumptions made in the model is related to the radial inhomogenity of the radiation and undulator fields. Off-axis electrons satisfy a different resonance condition than electrons close to the longitudinal axis since they experience a different undulator and radiation field. The main difference between the model and a fully 3D description of the electron beam is that this effect, which enters the source term indirectly, is taken into account in a density-averaged way. The electrons may be considered to move in an effectively $1\frac{1}{2}$D ponderomotive potential. Consequently, the model will be referred to as the $1\frac{1}{2}$D model in the remainder of this paper. As shown in [23], the model is valid as long as transverse gradients in the radiation field over the cross section $2\pi XY$ of the electron beam are small. Estimating the gradient length

of the radiation field by the cross section w_{nm}^2, this implies that the surface ratio $\xi_b = 2\pi XY/w_{nm}^2$ should be typically smaller then unity. Although the model has a wider range of applicability, in the next section an axisymmetric resonator configuration is considered in which an on-axis aperture is used to extract the radiation from the cavity.

III. APPLICATION TO A HOLE-COUPLED AXISYMMETRIC RESONATOR

The resonator consists of two circular, spherically curved mirrors, which are perfectly aligned. The hole is in either one of the mirrors. The radiation field can be considered to be axisymmetric $u(r, z, \bar{z})$, r being the cylindrical radius, when the interaction with the electron beam does not give rise to asymmetries. To this purpose, a FEL with a helical undulator is considered ($k_x = k_y = k_u/\sqrt{2}$). The electron pulses have equal emittance in both transverse directions $\epsilon = \epsilon_x = \epsilon_y$ and an axisymmetric Gaussian density profile proportional to e^{-r^2/R^2} where $X = Y = R/\sqrt{2}$. Note that also a planar undulator can be considered as long as betatron oscillations remain small.

Vacuum solutions of the paraxial equation can be obtained in terms of orthogonal Gauss-Laguerre (GL) modes [24] with common Rayleigh length l_R and waist position z_w (index $m = 0$ because of axisymmetry)

$$\Psi_{n0}(\xi, z) = \frac{s_0}{s} e^{-i\zeta_n} e^{-(1-i\alpha)\xi/2} L_n(\xi), \tag{11}$$

where $L_n(\xi)$ is the nth Laguerre polynomial with argument $\xi = 2r^2/s^2$, $s^2 = s_0^2(1+\alpha^2)$, $s_0^2 = 2l_R/k_0$ is the minimum spot size, $\alpha(z) = (z - z_w)/l_R$, and $\zeta_n(z) = (2n+1)\arctan\alpha$. The GL solutions describe an optical field with a spherical phase front. The radial extension of the GL modes is an increasing function of the mode number n. All GL modes are peaked on axis. Since the basis functions are explicitly known, the density-averaged function I_{n0} and the normalization w_{n0}^2, which enter the set of averaged equations (8) and (9), can be calculated. The result is

$$I_{n0} = \frac{1}{1+i\alpha+\xi_b}\left(\frac{1-i\alpha-\xi_b}{1+i\alpha+\xi_b}\right)^n \times\left[1+\frac{k_u^2R^2}{2}\left(\frac{1+\alpha^2-\xi_b(1-2n-i\alpha)}{1+\alpha^2-\xi_b^2+2i\alpha\xi_b}\right)\right] \tag{12}$$

with $w_{n0}^2 = \pi s_0^2/2$. The normalization is independent of the mode number and is equal to the minimum cross section of the optical field. The surface ratio $\xi_b = 2R^2(z,\bar{z})/s_0^2$ should be smaller than unity for the model to be valid. The second term in the square brackets in Eq. (12) arises from the radial dependence of the undulator field.

The reflection and transmission of the optical field by the cavity mirrors play an important role in a resonator FEL since multiple round-trips are required to reach saturation. When an aperture is used for power extraction, the radial structure of the optical field alters from pass to pass and affects the interaction between the optical field and electron beam by a change in the radial overlap of them. The reflection can be calculated analytically from the Huygens integral in the Fresnel approximation by expansion of both the incident and the reflected radiation fields into GL modes with Rayleigh length and waist position chosen such that the optical phase front exactly matches the radii of curvatures R_u and R_d of the "upstream" ($z = 0$) and "downstream" ($z = L_c$) mirrors [4]

$$z_w = \frac{(R_d - L_c)L_c}{R_u + R_d - 2L_c}, \quad l_R = \sqrt{z_w(R_u - z_w)}, \tag{13}$$

L_c being the cavity length. After reflection by the downstream and the upstream mirror, respectively, the radial profile of a radiation pulse at the exit of the undulator $\{u_m^{\rm out}\}$ is "scattered" into the radial mode structure $\{u_n^{\rm in}\}$ at the entrance of the undulator according to

$$u_n^{\rm in} = r_u r_d \sum_{k=0,m=0} e^{i\phi^{rt}(n,k,m)}\, \mathcal{R}_{nk}(0)\mathcal{R}_{km}(L_c)\, u_m^{\rm out}, \tag{14}$$

where the real coefficients r_u and r_d account for absorption loss due to a finite conductivity of each mirror and the round-trip phase

$$\phi^{\rm RT}(n,k,m) = 2k_0L_c - 2(m+k+1)\arctan\left(\frac{L_c - z_w}{l_R}\right) - 2(n+k+1)\arctan\left(\frac{z_w}{l_R}\right) \tag{15}$$

is related to the Guoy shift [5]. For both mirrors, positioned at $z = 0$ and $z = L_c$, scattering of the mode structure is determined by the reflection matrix

$$\mathcal{R}_{nm}(z) = \int_{\xi_{\rm MA}}^{\xi_{\rm MR}} d\xi\, e^{-\xi} L_n(\xi) L_m(\xi), \tag{16}$$

where the integral over ξ is calculated analytically using the recurrence relations of the Laguerre polynomials. The normalized aperture and radius of the mirror are given by $\xi_{\rm MA} = 2r_{\rm MA}^2/s^2$ and $\xi_{\rm MR} = 2r_{\rm MR}^2/s^2$, respectively. For given a resonator geometry, they depend on the radiation wavelength through the spot size of the optical field.

Note that when transmission loss is absent ($\xi_{\rm MA} \to 0$ and $\xi_{\rm MR} \to \infty$), e.g., in a closed resonator, the reflection coefficients reduce to $\mathcal{R}_{nm} = \delta_{nm}$. As a result, Eq. (14) simplifies to

$$u_n^{\rm in} = r_u r_d e^{i\phi^{RT}(n,n,n)} u_n^{\rm out}, \tag{17}$$

which demonstrates that, although the radiation amplitude changes according to the round-trip phase and the absorption coefficients, the distribution of radiation power proportional to $|u_n|^2$ over the radial modes is constant.

The extracted radiation power $P_{\rm out}$ is calculated from the energy density proportional to $|u|^2$ incident on the aperture rather than by using a transmission matrix ap-

proach similar to Eq. (14) since a large number of GL modes are required to described the outcoupled field. The result is

$$P_{\rm out} \propto (\pi s^2/2) \int_0^{\xi_{\rm MA}} d\xi \left| \sum_{n=0} u_n^i \frac{s_0}{s} e^{-i\zeta_n} e^{-(1-i\alpha)\xi/2} L_n \right|^2 = (\pi s_0^2/2) \sum_{n=0,m=0} \mathcal{R}_{nm} u_n^i u_m^{i*}, \quad (18)$$

where $\{u_n^i\}$ is the radiation field incident on the aperture and $\mathcal{R}_{nm}$ is given by Eq. (16) with $\xi_{\rm MA}$ and $\xi_{\rm MR}$ set to zero and to the aperture size, respectively.

IV. NUMERICAL RESULTS

In this section, results are presented that demonstrate the combined influence of the radial mode structure and of slippage effects on the evolution of an optical pulse in a hole-coupled, axisymmetric resonator FEL. The simulations are performed for the FEL parameters of Table I which are characteristic for FELIX [2]. The electron pulse has a parabolic profile $\mathcal{X} \propto 1 - (\bar{z}/2L_b)^2$ in the longitudinal direction, where L_b is the pulse length. The initial optical pulse is assumed to have the same longitudinal profile. For reasons of simplicity, the electron beam envelope R, the emittance ϵ, the initial energy detuning $\delta\gamma$, and the energy spread σ_e are assumed to be constant over the electron pulse. A matched beam is considered, $\epsilon/2\pi A_{u0} k_u R_0^2 = 1$. For a given emittance, this relation defines R_0. Furthermore, the energy detuning is optimized for the highest linear gain.

The electron beam consists of a train of electron pulses. The repetition rate of the electron pulses is such that the generated optical pulses do not interact and evolve independently. The cavity consists of two mirrors at distance L_c. A total power loss of 2.5% is assumed for absorption on both mirrors. This implies that $r_u = r_d = 0.994$. The aperture is in the upstream mirror. Furthermore, the center of the undulator is shifted with respect to the center of the cavity by an amount Δ_u, toward the downstream mirror.

TABLE I. Parameters used in the simulations.

Parameter	Symbol	Value
Basic FEL		
Undulator period	λ_u	0.065 m
Number of undulator periods	N_u	38
Initial electron energy	γ_0	46.3
Energy detuning	$\delta\gamma/\gamma_0$	1%
Energy spread	σ_e	0.35%
Normal emittance	ϵ	70π mm mrad
Peak current	I	75 A
Electron pulse length	L_b	0.60 mm
Cavity geometry		
Cavity length	L_c	6.00 m
Mirror curvature (upstream)	R_u	4.00 m
Mirror curvature (downstream)	R_d	3.00 m
Mirror radii	$r_{\rm MR}$	2.5 cm
Upstream mirror aperture	$r_{\rm MA}$	1.5 mm
Undulator shift	Δ_u	0.90 m

A. Cold cavity simulations

In the absence of an electron beam, the influence of the aperture and finite mirror size on the transverse structure $\{u_n\}$ of the radiation field is investigated by simulating an optical pulse which undergoes multiple reflections in the "cold" cavity. The radial profile of the optical pulse that evolves after a number of round-trips depends on the reflection matrix and on the initial radial mode structure. Convergent and reliable results are obtained with maximally five GL modes. The radiation wavelength is $\lambda_0 = 2\pi/k_0 = 20$ μm. Because transmission losses due to the finite mirror size (edge losses) are small at this wavelength, the off-diagonal elements of the upstream mirror originate mainly from scattering at the aperture. The reflection matrix of the downstream mirror is equal to a unity matrix $\mathcal{R}_{km}(L_c) = \delta_{km}$, to a good approximation. The initial optical pulse is chosen to be the $n = 0$ Gaussian radial mode.

The evolution of the radial mode structure is shown in Fig. 1. The initial Gaussian mode is scattered mainly into the *even* transverse modes $n = 2$ and $n = 4$. The energy scattered per pass into odd modes is as large as the one that is scattered into even modes. However, after a number of scattering events, their contribution is much smaller. This is related to the round-trip phase Eq. (15). For the specific geometry considered in this paper, the scattering of each mode n into itself yields a phase change that is proportional to $3\pi n$. Since the scattered energy originates from the Gaussian mode ($n = 0$), odd modes experience destructive phases each round-trip. Therefore, they alternately gain and lose energy. As a result,

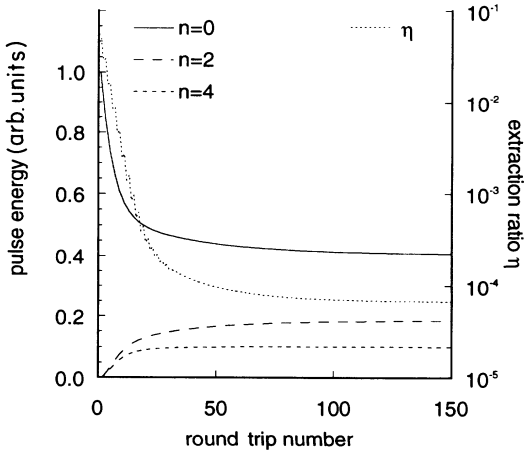

FIG. 1. The distribution of pulse-averaged energy over the radial modes and the extraction ratio η as a function of the round-trip number, showing the scattering of the initial radial profile into higher-order radial modes. Only the even modes $n = 0$, 2, and 4 are shown since the contribution of other modes is much smaller.

the net energy transferred to odd modes is much lower than to even modes, which are in phase each round-trip and add up coherently.

After approximately 50 round-trips, a nearly stationary configuration is reached in which the extraction ratio η, i.e., the ratio of extracted and intracavity pulse energies, is strongly reduced with respect to its initial value. In Fig. 2 the energy density distribution of the optical pulse at the beginning of the first round-trip and in the stationary region is shown. The results show that the mode composition of the optical field is changed such that the field intensity on axis is strongly reduced at the upstream mirror.

For longer wavelengths, edge losses become more important. These losses result in a reduction of the diagonal elements in the reflection matrix. The reduction is stronger for higher radial mode numbers n. Since at least two modes are required to create zero field intensity on axis, the screening of the aperture is effective as long as the reflection coefficient of the lowest even radial mode $n=2$ (besides $n=0$) is sufficiently large. For the parameters in Table I, the reflection coefficient $\mathcal{R}_{22}$ should be larger than 0.90, i.e., for $\lambda_0 < 40$ μm, as will be shown in Sec. IV B. For longer wavelengths, the radial mode structure consists mainly of the Gaussian mode, since all other modes are strongly reduced.

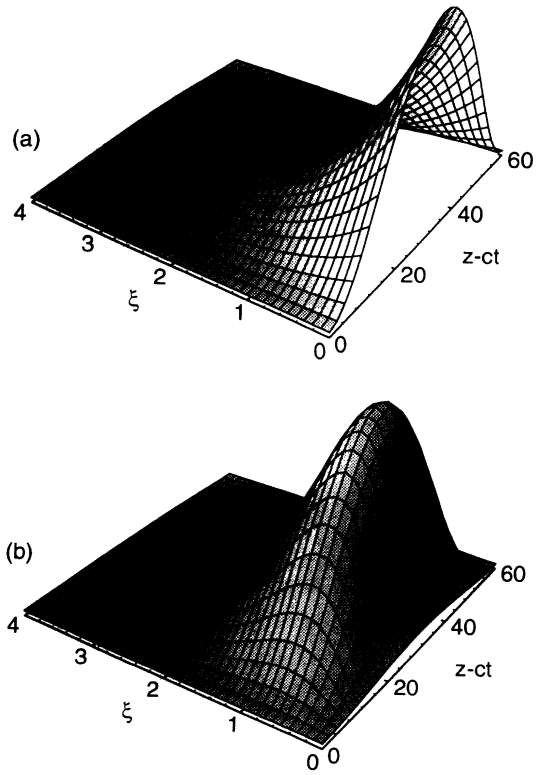

FIG. 2. The energy density of the optical pulse as a function of position $z - ct$ (in units of a wavelength λ_0) and radial coordinate $\xi = 2r^2/s^2$ (a) at the beginning of the first round-trip and (b) in the stationary region. The pulse is monitored just before the upstream mirror. The normalized radii of aperture and mirror are $\xi_{MA} = 0.057$ and $\xi_{MR} = 16.0$, respectively.

B. Multielectron simulations

In the presence of the electron pulse, the transverse and the longitudinal structure of the light pulse are determined, besides by aperture loss and scattering at the mirrors, by the amplification process due to the interaction and by the slippage with respect to the electron pulse. As pointed out in the Introduction, a shortening of the cavity leads to an effective synchronization of the light and electron pulses. The simulations presented here are performed at a fixed desynchronization $\Delta L = -2.0\lambda_0$, where $\Delta L = 0$ corresponds to synchronization. For this slightly shortened cavity, the gain of the optical field is close to its maximum value, as shown in Fig. 3. The effect of other values of ΔL will be discussed in a later stage.

The optical pulse has a parabolic longitudinal profile and consists of the Gaussian radial mode ($n = 0$). The wavelength is $\lambda_0 = 20$ μm, as in Sec. IV A. Starting from an initial power level of 0.1 W, the FEL operates in the linear regime up to approximately 50 round-trips. In this regime, a typical example of the energy density of the optical pulse and its decomposition into GL modes is shown in Fig. 4. The main fraction of the optical power overlaps with the electron pulse, which is located in the region $[0, 60]\lambda_{pon}$. Since there is a finite desynchronism, this implies that the group velocity of the optical field is reduced. The radial mode structure of the pulse consists mainly of the first three even-n GL modes of which the Gaussian mode ($n=0$) is dominant. Due to the gain, the energy density is concentrated near the axis. The largest values occur slightly off axis. This is due to the same mechanism that leads to screening of the mirror aperture when the electrons are absent. From a comparison with the cold cavity results in Figs. 1 and 2, one can conclude that, for the same number of round-trips, the transverse profile is dominated by the gain due to the interaction with the electron beam rather than by scattering due to the aperture.

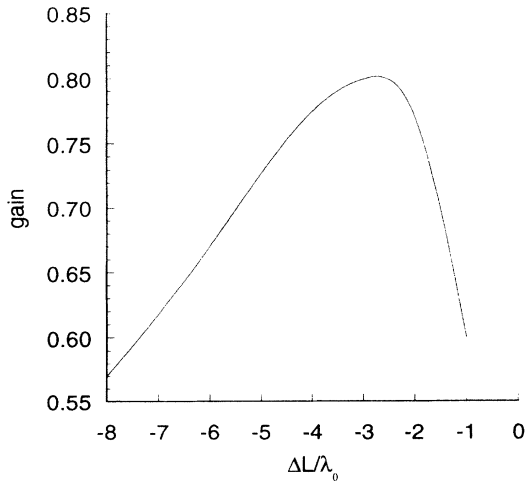

FIG. 3. Pulse-averaged linear gain (per pass) as a function of the desynchronization $\Delta L/\lambda_0$. The wavelength is $\lambda_0 = 20$ μm.

The evolution of the optical pulse in the saturated regime can be described as follows. First, due to the small gain, the effective velocity of the light pulse is increased. As a result, the optical pulse runs away more and more from the electron pulse, as shown in Figs. 5(a) and 5(b). In the subsequent round-trips, the electrons within a slippage length behind this first peak are affected by its high power level. In this region, a secondary peak is created, which consists mainly of the $n=2$ radial mode. The intracavity power of this peak remains much lower than the first peak because of a limited interaction time. Nevertheless, it gives a comparable contribution to the extracted power.

A slippage length behind the first peak, a new peak is generated which eventually grows as large as the first peak, as is shown in Figs. 5(c) and 5(d). The longitudinal and radial structure of this pulse is quite similar to those shown in Fig. 4. This is explained by the fact that the electrons near the trailing edge of the electron pulse have experienced only a low optical field and therefore radiate as if they were in the linear regime.

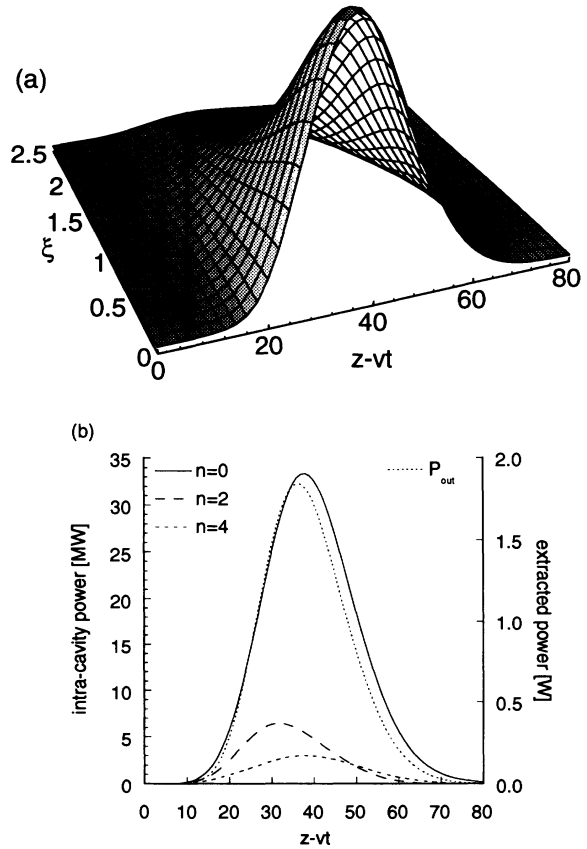

FIG. 4. (a) The energy density of the light pulse after ten round-trips, where the FEL operates in the linear regime, as a function of the longitudinal position $\bar{z} = z - v_{\rm pon}t$ (in units of $\lambda_{\rm pon}$) and the radial coordinate $\xi = 2r^2/s^2$. The pulse is monitored just before the upstream mirror. (b) Distribution of the radiation power over the radial modes and the extracted power as a function of the position in the pulse. The electrons are located in the region $[0, 60]\lambda_{\rm pon}$. Only the dominant modes are shown ($n = 0, 2$, and 4). The radiation wavelength is 20 μm and the normalized radii of aperture and mirror are as in Fig. 2.

This process is repeated periodically and leads to "limit-cycle" oscillations in the outcoupled power [25]. Figure 6 shows the energy density of the optical pulse near the end of the third cycle. The first two pulses are completely decoupled from the electron beam and propagate as in a cold cavity. The first pulse is already strongly reduced in amplitude due to mirror absorption loss. Their radial structure is influenced by mirror scattering only. In agreement with the results of the cold cavity simulations, a radial profile develops in which the on-axis field intensity is reduced. The radial mode structure of the two pulses differs from the result in Fig. 1, since they arise from radial profiles generated by the electrons.

For a desynchronization length with a more negative value, the separation between the pulses becomes larger. This implies that mirror scattering becomes more important. When the gain decreases, i.e., for $\Delta L < -4\lambda_0$, an additional narrowing of each pulse occurs.

These results are compared with results of a spatially 1D model [10], in which the radial profile of the optical pulse is characterized by a single number, the so-called filling factor. This factor is calculated assuming a Gaussian radial profile. In our model, which includes the full transverse structure of the optical field, it is found that the intracavity pulse energy is higher, although the extracted energy is considerably lower than in the 1D simulation. This is explained by the fact that a large fraction of the energy density is located off axis, as shown in this paper.

The scattering of the radial mode structure and the gain depend on the radiation wavelength. For the wavelength ranges 18–40 μm and 40–70 μm, Fig. 7 shows the extraction ratio η in comparison with the corresponding value from the 1D model. In the latter, η is equal to the $\mathcal{R}_{00} = 1 - e^{-\xi_{MA}}$ element of the matrix in Eq. (18). The wavelength scan is obtained by changing the undulator strength A_{u0} while keeping other parameters fixed. The calculations are performed for a fixed desynchronization length ΔL, optimized for maximum gain at the lowest wavelength in each range. The extraction ratio is significantly lower than that of the 1D model, for wavelengths up to approximately 32 μm. For these short wavelengths, the extraction ratio depends strongly on the radial mode structure of the light. The irregularity in this range is related to the radial profile, which is due to the combined effect of the undulator strength, slippage, desynchronization, and scattering at the mirrors, which all depend on the wavelength. These effects can result in small changes in the relative phases of the radial mode structure inside the cavity and can lead to significant changes in the outcoupled power. For longer wavelengths $\lambda_0 \geq 40$ μm, the mode structure consists mainly of the Gaussian mode, which is due to the increased losses of higher-order modes. As a consequence, the effective screening of the aperture is strongly diminished. Higher-order GL modes are still residually present since they are generated by the electrons each pass.

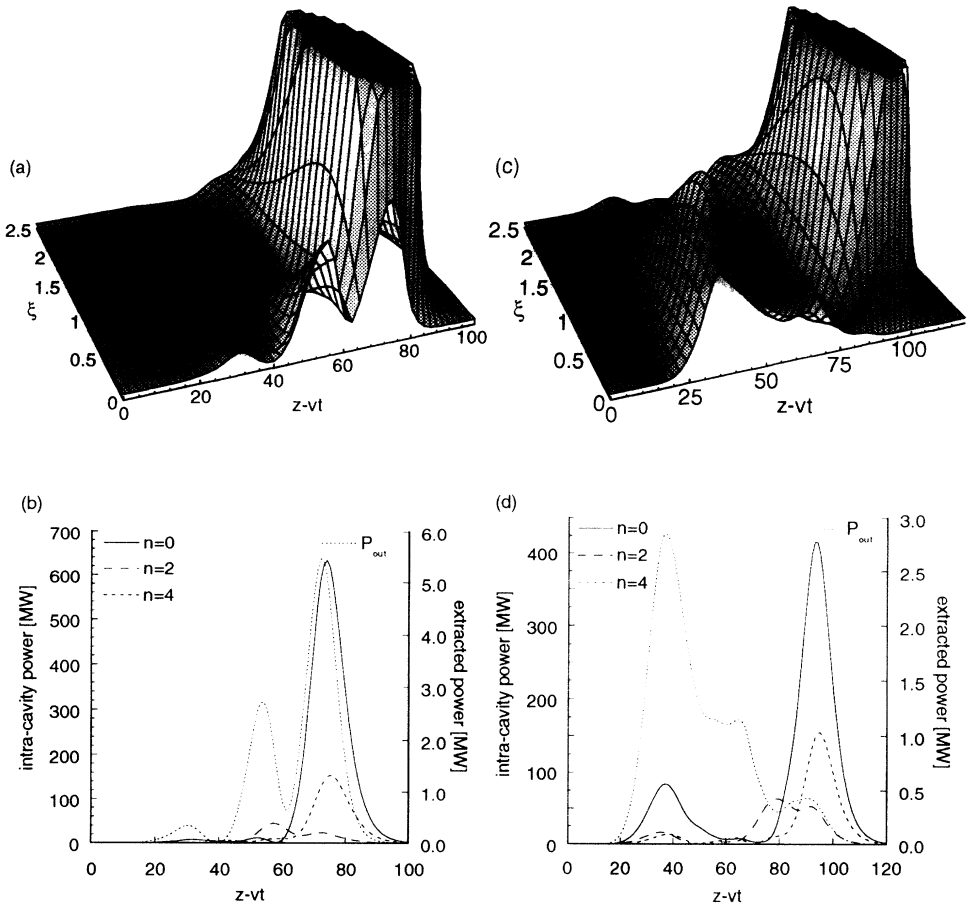

FIG. 5. First two cycles (a) and (b) after 60 round-trips and (c) and (d) after 70 round-trips of the pulse evolution after saturation is reached. The large peak energy density of the first pulse in (a) and (c) is cut off artificially. All parameters are similar to Fig. 4.

V. CONCLUSIONS

In a hole-coupled resonator FEL, which employs a continuous electron beam as gain medium, the radial profile of the optical field inside the cavity is determined by the amplification process, by power loss through the aperture, and by scattering at the mirrors. In pulsed beam operation, the additional effect of slippage couples the radial and longitudinal structure of the light pulse.

In this paper, we have analyzed the spatial structure of the optical pulse inside the cavity and the fraction of power lost through the aperture. In the linear regime of FEL operation, the optical pulse is confined to the electron pulse. The transverse field structure consists mainly of the $n = 0$ Gaussian radial mode with its maximum amplitude on axis. After saturation has been reached, the light pulse overtakes the electrons and eventually does not interact with the electrons any more. In this cold cavity region, a substantial fraction of the radiation intensity of the Gaussian mode is transferred to the higher-order GL modes $n = 2$ and $n = 4$. For the cavity geometry investigated in this paper, the contribution of odd modes is small. The mode composition yields a radial profile in which the on-axis field strength is significantly reduced. Consequently, this screening of the aperture leads to a decrease of the extraction ratio as compared to the extraction ratio of the Gaussian mode created by the amplification process. Behind this first pulse, a new pulse is generated by the electrons as in the linear gain regime. In subsequent round-trips, the new pulse will saturate and evolve in a similar manner as the first pulse. After a number of such cycles, the field consists of a train of pulses. Only the energy density of the last pulse, which partially overlaps with the electrons, is concentrated on axis.

The effective screening of the mirror aperture can reduce the extraction ratio by one order of magnitude as compared with the extraction ratio of a Gaussian radial profile. The creation of higher-order GL modes, leading to the screening effect, can only occur for small values of the wavelength such that transmission losses due to the finite mirror size are small. For longer wavelengths, the higher-order GL modes lose most of their energy at

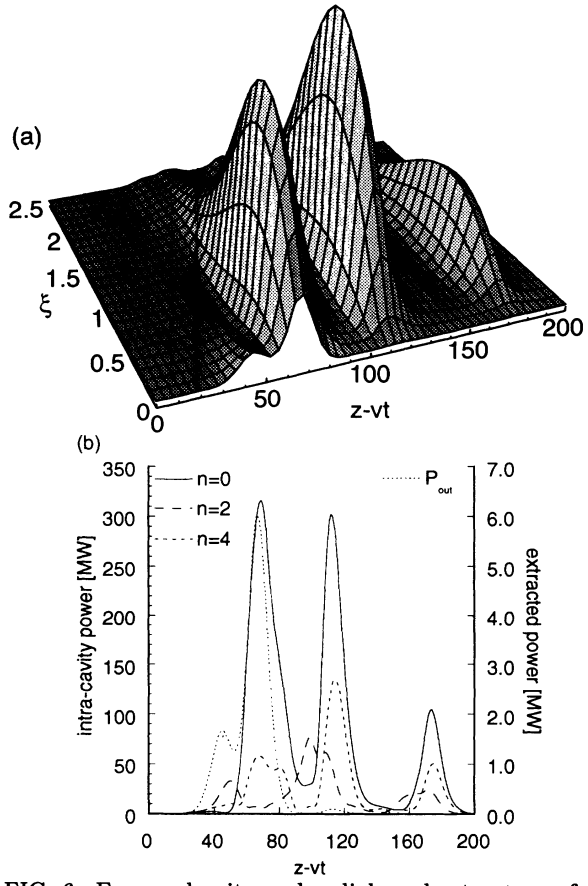

FIG. 6. Energy density and radial mode structure of the optical pulse after 110 round-trips, near the end of the third cycle. All parameters are similar to Fig. 4.

the mirror edge since the radial extension of the modes increases with the mode number. Eventually, only the Gaussian profile remains and the simulation results approach those obtained with a spatially 1D model.

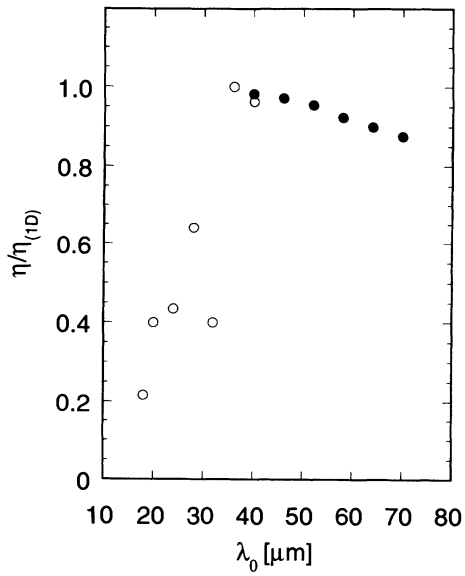

FIG. 7. The extraction ratio η relative to the corresponding value from a spatially one dimensional model, as a function of wavelength. The open and solid circles correspond to different initial electron energies $\gamma_0 = 46.3$ and $\gamma_0 = 34.5$, respectively.

ACKNOWLEDGMENTS

The authors are indebted to Dr. Ir. R.J. Bakker, Dr. G. Knippels, and Dr. D. Oepts for helpful discussions. This work was performed as part of the research program of the Stichting voor Fundamenteel Onderzoek der Materie with financial support from the Nederlandse Organisatie voor Wetenschappelijk Onderzoek. One of the authors (B.F.) is supported by the European Infrared FEL Network (Contract No. CHRX-CT93-0109).

[1] T.C. Marshall, *Free Electron Lasers* (MacMillan, New York, 1985).
[2] R.J. Bakker, C.A.J. van der Geer, D.A. Jaroszynski, A.F.M. van der Meer, D. Oepts, P.W. van Amersfoort, V. Anderegg, and P.C. van Son, Nucl. Instrum. Methods A **331**, 79 (1993).
[3] S. Riyopolous, P. Sprangle, C.M. Tang, and A. Ting, Nucl. Instrum. Methods A **272**, 543 (1988).
[4] B. Faatz, R.W.B. Best, D. Oepts, and P.W. van Amersfoort, IEEE J. Quantum Electron. **QE-29**, 2229 (1993).
[5] G.A. Barnett, S.V. Benson, and J.M.J. Madey, IEEE J. Quantum Electron. **QE-29**, 479 (1993).
[6] R. Bonifacio, C. Pellegrini, and L.M. Narducci, Opt. Commun. **50**, 373 (1984).
[7] W.B. Colson, Phys. Quantum Electron. **8**, 457 (1982).
[8] G.T. Moore and N. Piovella, IEEE J. Quantum Electron. **QE-27**, 2522 (1991).
[9] R. Bonifacio, L. De Salvo Souza, P. Pierini, and N. Piovella, Nucl. Instrum. Methods A **292**, 358 (1990).
[10] W.B. Colson, Nucl. Instrum. Methods A **250**, 168 (1986).
[11] T.-M. Tran and J.S. Wurtele, Comput. Phys. Commun. **54**, 263 (1989).
[12] J.E. La Sala, D.A.G. Deacon, and T.E. Scharlemann, Nucl. Instrum. Methods A **250**, 19 (1986).
[13] S.Y. Cai, A. Bhattacharjee, and T.C. Marshall, Nucl. Instrum. Methods A **272**, 481 (1988).
[14] C.M. Tang and P.A. Sprangle, IEEE J. Quantum Electron. **QE-21**, 970 (1985).
[15] P.A. Sprangle, A. Ting, and C.M. Tang, Phys. Rev. Lett. **59**, 202 (1987).
[16] G. Dattoli, Honglie Fang, A. Torre, and R. Caloi, IEEE J. Quantum Electron. **QE-28**, 901 (1992).
[17] J. Blau and W.B. Colson, Nucl. Instrum. Methods A **318**, 717 (1992).
[18] L.A. Weinstein, *Open Resonators and Open Waveguides* (Golem, Boulder, 1969).
[19] R.E. Aamodt, Phys. Rev. A **40**, 5058 (1989).
[20] A.E. Siegman, *Lasers* (University Science, Mill Valley,

CA, 1986).
[21] P. Jha and J.S. Wurtele, Nucl. Instrum. Methods A **331**, 477 (1993).
[22] K.G. Steffen, *High Energy Beam Optics* (Wiley Interscience, New York, 1965).
[23] G.H.C. van Werkhoven, B. Faatz, and T.J. Schep, Nucl. Instrum. Methods A **331**, 411 (1993).
[24] A. Yariv, *Introduction to Optical Electronics* (Holt, Rinehart and Winston, New York, 1971).
[25] D.A. Jaroszynski, R.J. Bakker, D. Oepts, A.F.G. van der Meer, and P.W. van Amersfoort, Nucl. Instrum. Methods A **331**, 52 (1993).

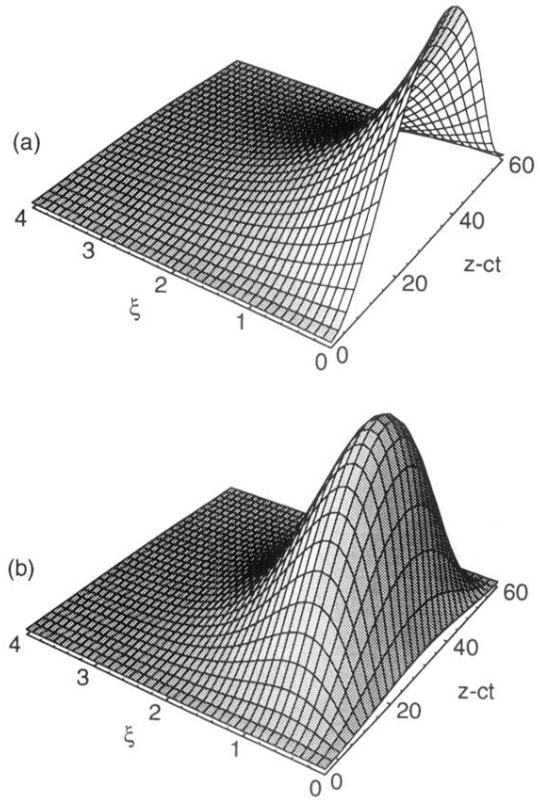

FIG. 2. The energy density of the optical pulse as a function of position $z - ct$ (in units of a wavelength λ_0) and radial coordinate $\xi = 2r^2/s^2$ (a) at the beginning of the first round-trip and (b) in the stationary region. The pulse is monitored just before the upstream mirror. The normalized radii of aperture and mirror are $\xi_{\mathrm{MA}} = 0.057$ and $\xi_{\mathrm{MR}} = 16.0$, respectively.

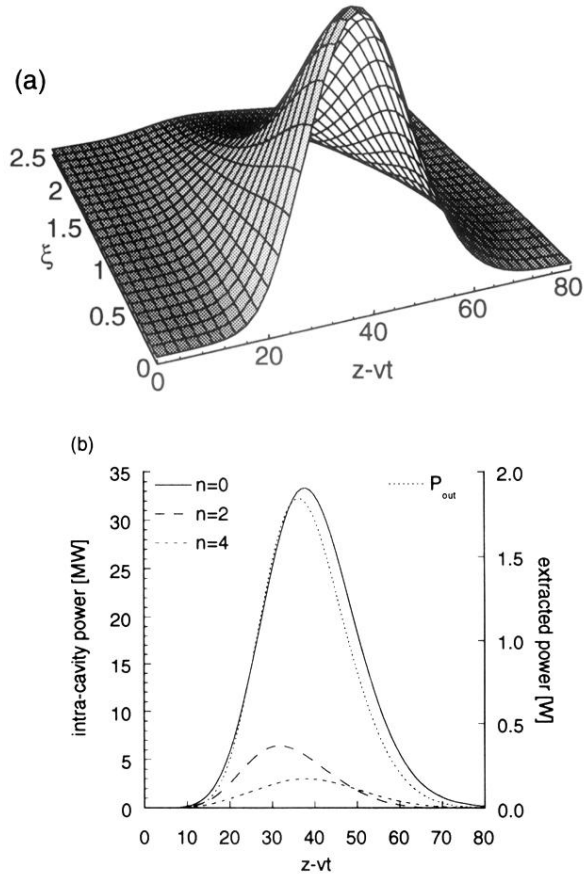

FIG. 4. (a) The energy density of the light pulse after ten round-trips, where the FEL operates in the linear regime, as a function of the longitudinal position $\bar{z} = z - v_{\mathrm{pon}} t$ (in units of λ_{pon}) and the radial coordinate $\xi = 2r^2/s^2$. The pulse is monitored just before the upstream mirror. (b) Distribution of the radiation power over the radial modes and the extracted power as a function of the position in the pulse. The electrons are located in the region $[0, 60]\lambda_{\mathrm{pon}}$. Only the dominant modes are shown ($n = 0, 2$, and 4). The radiation wavelength is 20 μm and the normalized radii of aperture and mirror are as in Fig. 2.

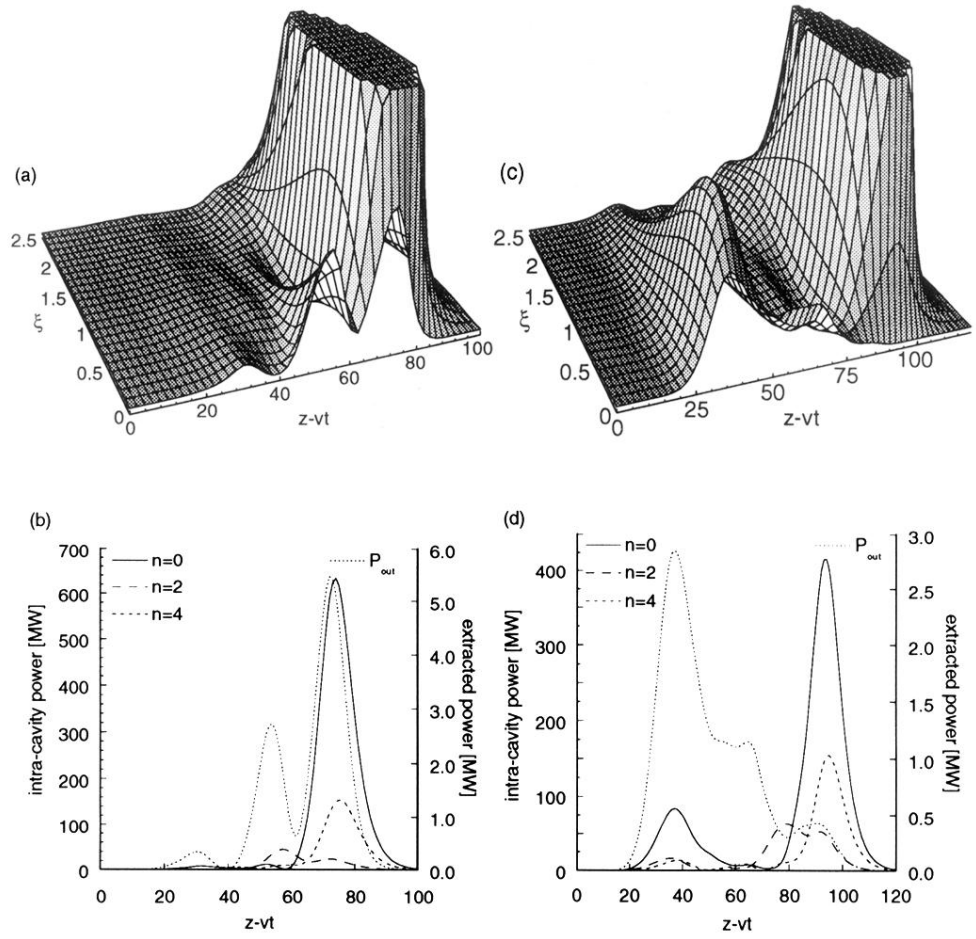

FIG. 5. First two cycles (a) and (b) after 60 round-trips and (c) and (d) after 70 round-trips of the pulse evolution after saturation is reached. The large peak energy density of the first pulse in (a) and (c) is cut off artificially. All parameters are similar to Fig. 4.

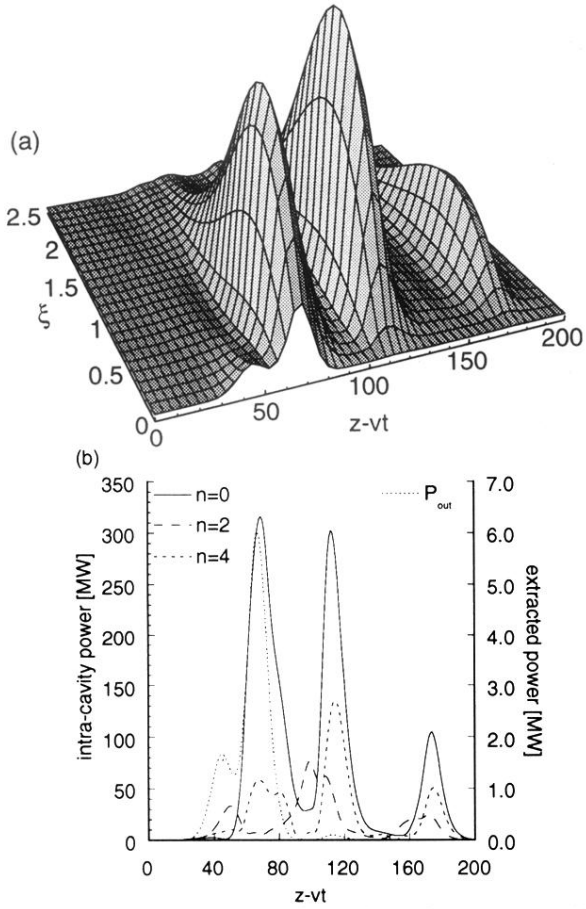

FIG. 6. Energy density and radial mode structure of the optical pulse after 110 round-trips, near the end of the third cycle. All parameters are similar to Fig. 4.